1986

NASA/ASEE SUMMER FACULTY FELLOWSHIP PROGRAM

MARSHALL SPACE FLIGHT CENTER
THE UNIVERSITY OF ALABAMA

SHARPLY CURVED TURN AROUND DUCT FLOW PREDICTIONS USING SPECTRAL PARTITIONING OF THE TURBULENT KINETIC ENERGY AND A PRESSURE MODIFIED WALL LAW

Prepared By:	L. Michael Santi, Ph.D.
Academic Rank:	Assistant Professor
University and Department:	Memphis State University Mechanical Engineering
NASA/MSFC: Laboratory: Division: Branch:	 Systems Dynamics Atmospheric Sciences Computational Fluid Dynamics
MSFC Counterpart:	Charles Schafer
Date:	August 28, 1986
Contract No:	NGT 01-002-099 The University of Alabama

SHARPLY CURVED TURN AROUND DUCT FLOW PREDICTIONS USING SPECTRAL PARTITIONING OF THE TURBULENT KINETIC ENERGY AND A PRESSURE MODIFIED WALL LAW

BY

L. Michael Santi
Assistant Professor of Mechanical Engineering
Memphis State University
Memphis, Tennessee

ABSTRACT

Computational predictions of turbulent flow in sharply curved 180 degree turn around ducts are presented. The CNS2D computer code developed at Marshall Space Flight Center is used to solve the equations of motion for two-dimensional incompressible flows transformed to a nonorthogonal body-fitted coordinate system. This procedure incorporates the pressure velocity correction algorithm SIMPLE-C to iteratively solve a discretized form of the transformed equations. A multiple scale turbulence model based on simplified spectral partitioning is employed to obtain closure. Flow field predictions utilizing the multiple scale model are compared to features predicted by the traditional single scale k-ε model. Tuning parameter sensitivities of the multiple scale model applied to turn around duct flows are also determined.

In addition, a wall function approach based on a wall law suitable for incompressible turbulent boundary layers under strong adverse pressure gradients is tested. Turn around duct flow characteristics utilizing this modified wall law are presented and compared to results based on a standard wall treatment.

LIST OF FIGURES

NOMENCLATURE

SYMBOL	DIFINITION
C_1	production constant in ss k-ε turbulence model (=1.44, see equation (5))
C_2	dissipation rate constant in ss k-ε turbulence model (=1.92, see equation (5))
C_{p1}	production constant in ε_p transport relation (=1.6, see equation (9))
C_{p2}	dissipation rate constant in ε_p transport equation (see equation (9))
C_{t1}	spectral transport constant in ε_t transport equation (=1.15, see equation (10))
C_{t2}	dissipation rate constant in ε_t transport equation (see equation (10))
C_μ	diffusivity constant in two-equation models (=0.09, see equation (3))
D	duct width
k	turbulent kinetic energy
k_p	large eddy turbulent kinetic energy (see Figure 2)
k_t	intermediate spectral range turbulent kinetic energy (see Figure 2)
K_1	large eddy upper wave number limit (see Figure 2)
K_2	dissipative range lower wave number limit (see Figure 2)
P_e	inlet plane pressure
P_r	turbulent energy production term (see equation (6))
R_c	TAD centerline radius of curvature
t	time
u	x-directed velocity component, or TAD longitudinal velocity component
u^+	dimensionless universal velocity
$\overline{u_i u_j}$	Reynolds stress component

SYMBOL	DEFINITION
U	time average longitudinal velocity
$\overline{U}$	duct average longitudinal velocity
v	y directed velocity component, or TAD spanwise velocity component
v^*	friction velocity
x	Cartesian coordinate direction
y	Cartesian coordinate direction
y^+	dimensionless y ($=yv^*/\nu$)
ε	turbulent kinetic energy dissipation rate
ε_p	large eddy dissipation in the cascade
ε_t	intermediate range eddy dissipation in the cascade
η	spanwise coordinate in BFC transformed system
θ	angle measured from TAD inlet plane
μ	absolute viscosity
μ_{eff}	effective total viscosity ($=\mu+\mu_t$)
μ_t	effective turbulent viscosity in Boussinesq approximation
ν	kinematic viscosity
ν_t	kinematic turbulent viscosity
ξ	longitudinal coordinate in BFC transformed system
ρ	density
σ_{k_p}	large eddy turbulent kinetic energy Prandtl number
σ_{k_t}	intermediate range eddy kinetic energy Prandtl number
σ_{ε_p}	large eddy dissipation rate Prandtl number

SYMBOL	DEFINITION
σ_{ε_t}	intermediate range eddy dissipation rate Prandtl number
ψ	stream function
Re	Reynolds number
CFD	computational fluid dynamics
BFC	body-fitted coordinates
SIP	Stone's implicit procedure
SSME	space shuttle main engine
TDMA	tridiagonal matrix solver
ms k-ε	multiple-scale k-ε model
ss k-ε	conventional single-scale k-ε model
mwf	pressure modified wall function
*	superscript denoting dimensionless quantity

I
INTRODUCTION

The limitations of current "state of the art" turbulence models are quickly realized when applied in conjunction with computational fluid dynamic (CFD) analysis of typical turbomachine flow configurations. The tortuous nature of the flow path as well as the occurrence of complex phase and composition changes present obstacles that preclude totally satisfactory modeling.

Much attention has been directed toward turbulence model improvements based upon the incorporation of additional pressure strain effects and/or wall contributions in streamfields with significant curvature [1-9]. Due to the computational complexity of CFD analyses applied to typical turbomachine configurations, and to the inherent limitations of the popular k-ε model upon which most curvature modified constitutive relations are based, there is no general consensus on the desirability of any specific curvature modified model.

Several numerical methods utilizing body-fitted coordinates have been developed which are suitable for solving the incompressible Navier-Stokes equations in complex passageways [10-14]. Each method employs a specific strategy for determining the pressure field such that the flow field is divergence free. Although there are many heuristics associated with these CFD techniques, it is apparent that sufficiently robust computational strategies are now available for analysis of complex, curvature-dominated flow regimes. It is, therefore, obvious that accuracy of turbulent flow prediction depends largely on the quality of the turbulence model.

Recently, several turbulence models have been developed [15-18] which address the most serious drawback of two-equation closure models, namely, the characterization of the whole spectrum of turbulent motion by a single set of scales. This simplification inherently assumes equilibrium spectral energy transfer and can be appropriately applied only to cases where the mean flow evolves slowly. This type of flow condition almost never exists in typical turbomachine applications. The modest successes of two-equation models in predicting complex curvature dominated flows is more a testimony to the perseverance of researchers in this arena and the demand driven development of computational heuristics to accomodate experimental observation than to any inherent physical applicability.

The so-called "multiple-scale" turbulence models feature a two regime partition of the energy spectrum. The turbulence properties associated with large scale energetic vortices are related to mean velocity gradients while the turbulence dissipation occurring primarily in small scale eddies is related to energy transfer by its own action rather than to the overall kinetic energy.

In section III of this report, a brief outline of a specific multiple-scale model developed in reference [18] is presented. This turbulence model, as implemented in the SIMPLE-C based computer code [14] developed at Marshall Space Flight Center, was applied to analyze high rate turbulent flows in the two-dimensional turn around duct (TAD) configuration described in Figure 1. The sharply curved section of this geometry is characteristic of the space shuttle main engine (SSME) fuel side turbopump TAD. In addition, this configuration is reasonably representative of general, curvature dominated, internal flows and as such provides a meaningful test case for measuring the predictive capability of the specific multiple-scale turbulence model employed.

Computationally derived TAD flow predictions generated using the CNS2D implementation of the twin scale turbulence model are compared to results obtained using the standard k-ε model and to results obtained using a curvature modified wall function [9] in conjunction with the traditional k-ε model in section IV. In all analyses, the widely used wall function approach is used for the treatment of near wall boundary conditions [19,20] in order to achieve computational efficiency.

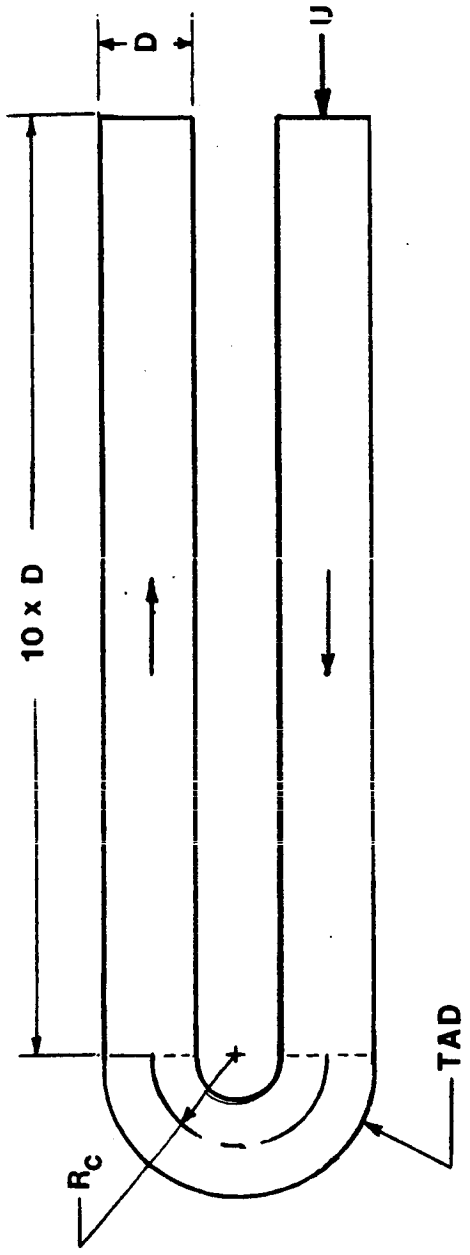

Figure 1. Geometric configuration for TAD analyses.

II
OBJECTIVES

The general objectives of this investigation are threefold. Contributions to the data base of computational results involving curvature dominated flows are to be provided. Secondly, comparisons of computationally derived results utilizing several turbulence model modifications are to be cataloged in order to test the sensitivity of flow prediction to turbulence model. Finally, a tentative evaluation of parent CFD code reliability and robustness is sought by quantitative comparison with experimental results and by qualitative comparison with previous computational results and extrapolated experimentation.

The specific objectives of this study are listed below.

1) To provide computational predictions of TAD flow field characteristics at high flow rates utilizing the CNS2D computer code.

2) To study flow field predictions obtained by using the multiple-scale turbulence model within the CNS2D computer implementation.

3) To study the effects of a modified wall function treatment on TAD flow predictions at very large flow rates.

4) To compare the phenomenological characteristics of TAD flows provided by the multiple-scale turbulence model with the predictions of traditional two-equation models.

5) To estimate tuning parameter sensitivity of the specific multiple-scale turbulence model employed.

III
BACKGROUND

The CNS2D computer code was developed by Y. S. Chen at NASA's Marshall Space Flight Center. It provides a numerical procedure for solving the discretized equations of motion for two-dimensional flows utilizing nonorthogonal body-fitted coordinate (BFC) systems. The equations of motion are transformed to a curvilinear coordinate system appropriate to the geometric configuration under analysis. For complex geometries, individual cells defined by the spatial grid discretization of the problem are locally transformed into regular 0-1 square volumes in (ξ,η) space by means of a bilinear transformation. For incompressible Newtonian fluids, the motion governing equations in Cartesian coordinates can be written as

$$E_x + F_y = S \tag{1}$$

where

$$E = \begin{Bmatrix} \rho u \\ \rho uu - \mu u_x \\ \rho uv - \mu v_x \end{Bmatrix} \qquad F = \begin{Bmatrix} \rho v \\ \rho uv - \mu u_y \\ \rho vv - \mu v_y \end{Bmatrix}$$

$$S = \begin{Bmatrix} 0 \\ (\mu u_x)_x + (\mu v_x)_y - P_x \\ (\mu u_y)_x + (\mu v_y)_y - P_y \end{Bmatrix}$$

In the (ξ,η) transform domain these equations become

$$E_\xi \xi_x + E_\eta \eta_x + F_\xi \xi_y + F_\eta \eta_y = S(\xi,\eta). \tag{2}$$

The metrics ξ_x, η_x, ξ_y, and η_y are computed numerically using second order central differencing.

For turbulent flow calculations, the molecular viscosity in these equations is replaced by an effective viscosity $\mu_{eff} = \mu + \mu_t$, where $_t$ is an effective turbulent viscosity introduced via the Boussinesq approximation. The turbulent viscosity must be supplied by appealing to an appropriate turbulence model. In the popular k-ε model, μ_t is related to the turbulent kinetic energy, k, and its dissipation rate, ε, by the expression [19]

$$\mu_t = \rho C_\mu k^2/\varepsilon . \tag{3}$$

where k and ε must themselves satisfy differential transport equations

of the form

$$(\rho U_i k - \mu_{eff} k_{x_i}/\sigma_k)_{x_i} = \rho(P_r - \varepsilon) \tag{4}$$

$$(\rho U_i - \mu_{eff} \varepsilon_{x_i}/\sigma_\varepsilon)_{x_i} = \rho(C_1 P_r - C_2 \varepsilon)\varepsilon/k \tag{5}$$

In the above equation the kinetic energy production term is given by the relation

$$P_r = C_\mu (k^2/\varepsilon) \; [(u_y+v_x)^2 + 2(u_x^2+v_y^2)] \tag{6}$$

and the model constants are generally accepted to be approximately

$$C_\mu = 0.09 \qquad \sigma_k = 1.00 \qquad \sigma_\varepsilon = 1.30$$

$$C_1 = 1.44 \qquad C_2 = 1.92$$

based on experimentation.

Solution of the (ξ,η) transformed version of equations (1),(4), and (5), in discretized form, is obtained iteratively by using the pressure velocity correction algorithm, SIMPLE-C [21]. Second order upwinding is used to approximate the convective terms. A grid staggering scheme, described in detail in reference [14], is employed to remove the difficulty in solving the Poisson pressure correction equation which couples the pressure and velocity fields. The system of algebraic equations arising from the discretization process is solved using a combination of the tridiagonal matrix solver (TDMA) [22] and Stone's implicit procedure (SIP) [23]. The wall boundary approach is used for the treatment of near wall boundary conditions.

If the inherent computational limitations of the well tested SIMPLE based algorithmic approach are accepted as a necessary price for meaningful approximation of complex fluid flows, then improvements in predictive capability must come either from improved turbulence models or from modified wall boundary treatments. In the context of two-equation turbulence closure models, a single time scale is used to characterize all turbulent motions. Because turbulence comprises fluctuating motions with a spectrum of sizes and time scales, it is obvious that mathematical models providing a single time scale are fundamentally limited. Therefore, the motivation for multiple-scale modeling is readily apparent.

The theoretical basis for the multiple-scale model employed in this study is described in detail by Hanjalic et al. [16]. A typical

energy spectrum for shear flow at high Reynolds numbers is displayed in Figure 2. The quantities K_1 and K_2 in this figure denote respectively the wave number above which no significant mean strain production occurs and the largest wave number at which the viscous dissipation of turbulence energy is unimportant. Energy leaves the "production" region ($K < K_1$) at a rate ε_p and enters the "dissipation" region ($K > K_2$) at a rate ε. Between these regions is an intermediate range of wave numbers in the so-called "transfer" region with a representative spectral energy transfer rate ε_t.

Although the description provided by Figure 2 is simplistic, it does provide for zonal shape changes in the energy spectrum whereas traditional single-scale models inherently assume spectral equilibrium with $\varepsilon_p = \varepsilon_t = \varepsilon$. Recognizing that sharply curved internal flows are susceptible to significant recirculation with a high degree of spectral nonequilibrium, the potential for turbulence model improvement using a multiple-scale concept is apparent.

In order to utilize the multiple-scale concept in a manner analagous to the two-equation model approach, it is necessary to develop transport equations for k_p, k_t, ε_p, and ε_t. It is assumed that spectral equilibrium exists between the transfer region and dissipative region, i.e. $\varepsilon = \varepsilon_t$.

For practical applications the gradient formulation suggested by Launder and Spalding [19] was employed by Chen [18]. The model transport equations are thus given by the relations

$$\frac{Dk_p}{Dt} = \frac{\partial}{\partial x_j}\left(\frac{\nu_t}{\sigma_{k_p}}\frac{\partial k_p}{\partial x_j}\right) + P_r - \varepsilon_p \tag{7}$$

$$\frac{Dk_t}{Dt} = \frac{\partial}{\partial x_j}\left(\frac{\nu_t}{\sigma_{k_t}}\frac{\partial k_t}{\partial x_j}\right) + \varepsilon_p - \varepsilon_t \tag{8}$$

$$\frac{D\varepsilon_p}{Dt} = \frac{\partial}{\partial x_j}\left(\frac{\nu_t}{\sigma_{\varepsilon_p}}\frac{\partial \varepsilon_p}{\partial x_j}\right) + \frac{\varepsilon_p}{k_p}\left(C_{p1}P_r - C_{p2}\varepsilon_p\right) \tag{9}$$

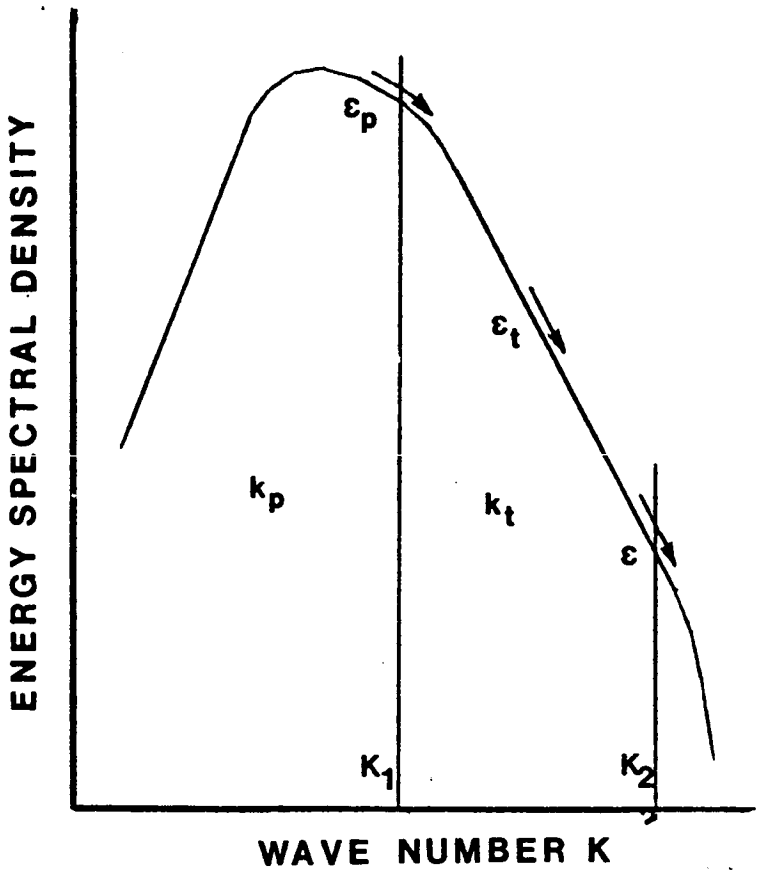

Figure 2. Energy Spectrum for multiple scale k-ε model. See reference [16].

$$\frac{D\varepsilon_t}{Dt} = \frac{\partial}{\partial x_i}\left(\frac{\nu_t}{\sigma_{\varepsilon_t}}\frac{\partial \varepsilon_t}{\partial x_i}\right) + \frac{\varepsilon_p}{k_p}\left(C_{t1}\varepsilon_p - C_{t2}\varepsilon_t\right) \qquad (10)$$

In equations (7) through (10), the first term on the right hand side obviously represents the flux of the respective turbulence property by diffusion. P_r is the rate of production of kinetic energy by mean velocity gradients (see equation (6)), ε_p is the energy transfer rate from the large scale disturbances to smaller scale eddies in the cascade, and ε_t is the flux of energy through the "transfer" region into the "dissipation" range. The time scale k_p/ε_p used in equations (9) and (10) has the property that when $\varepsilon_p = \varepsilon_t = \varepsilon$, the multiple-scale model recovers the single-scale k-ε model [18].

Development of the model coefficients appearing in equations (7) through (10) is detailed in reference [18]. These are given below.

$$\sigma_{k_p} = \sigma_{k_t} = 1$$

$$\sigma_{\varepsilon_p} = \sigma_{\hat{\varepsilon}_t} = 1.22$$

$$C_{p1} = 1.6 \qquad C_{p2} = 1.8 - 0.3\,[1-k_t/k_p]/[1+k_t/k_p]$$

$$C_{t1} = 1.15 \qquad C_{t2} = 1.8\,\varepsilon_t/\varepsilon_p$$

The value of C_{p2}, dependent upon the ratio k_t/k_p, is especially important for it is here that cross-talk between intermediate range disturbances and the large scale eddies is introduced. If C_{p2} were chosen to be a constant, the transport equation for ε_p would be largely independent of the intermediate scale motions since neither ε_t nor k_t would explicitly appear. The form of C_{p2} given above was chosen by Hanjalic et al. [16] and modified by Chen [18] in order to best agree with a variety of test flow data. In the context of the gradient diffusion Boussinesq type approximation, the suggested form of the eddy viscosity is expressed as [18]

$$\nu_t = C_\mu\,(k_p + k_t)\,k_p/\varepsilon_p \qquad (11)$$

where k_p/ε_p is used in place of k/ε as the appropriate time scale.

It should be noted that additional production terms due to extra strain rate appear in the $D\overline{u_i u_j}/Dt$ term of the Reynolds stress transport equations when body-fitted coordinates are employed in the analysis of curved shear flows [5,27]. These terms cannot be neglected and traditionally are included in the energy production rate term. In the (ξ,η) transformation domain, the rate of kinetic energy production would then be represented by the transformed version of equation (6) plus production terms due to extra strain which properly arise in the expression for Dk/Dt. This heuristic production increase is not included in the CNS2D computer code. The formal transformation represented by equation (2) is rigorously applied to all transport relations. The effect of the absence of these so-called extra strain production terms on the computational results that follow cannot be assessed without further investigation.

The multiple-scale turbulence model provides a particularly simple method for potential improvement in the computational prediction of turbulent flows by incorporating a degree of spectral information. However, improper application of conventional wall functions to turbulent boundary layers under adverse pressure gradients contributes to the discrepancies observed between computational predictions and experimental measurements. Despite this, the logarithmic law velocity profile remains the conventional method of providing boundary conditions for the governing transport equations of turbulent motion. The inadequacy of this profile assumption for increasingly large adverse pressure gradients is graphically depicted in Figure 3. In the context of a wall function approach it is necessary to utilize a wall law more reflective of the profile characteristics exhibited in Figure 3 in order to successfully predict the flow field properties occurring in typical turbomachine applications.

Several such modified wall treatments have been proposed [8,9,24,25]. Recently Nakayama and Kato [8] derived a wall law, including the effects of adverse pressure gradients, from a one-dimensional analysis of the turbulent kinetic energy equation with gradient diffusion employed to model the near wall shear stress variation. This approach was modified by Chen [9] and incorporated as an option in the CNS2D computer code. Details of this procedure are quite complex and the reader is referred to references [8,9] for a complete development.

In section IV of this report, TAD flow predictions are examined using a traditional k-ε turbulence model with a conventional wall treatment developed by Chen [9]. Comparisons with results of TAD analysis using the multiple-scale turbulence model are presented and phenomenological differences in prediction are displayed.

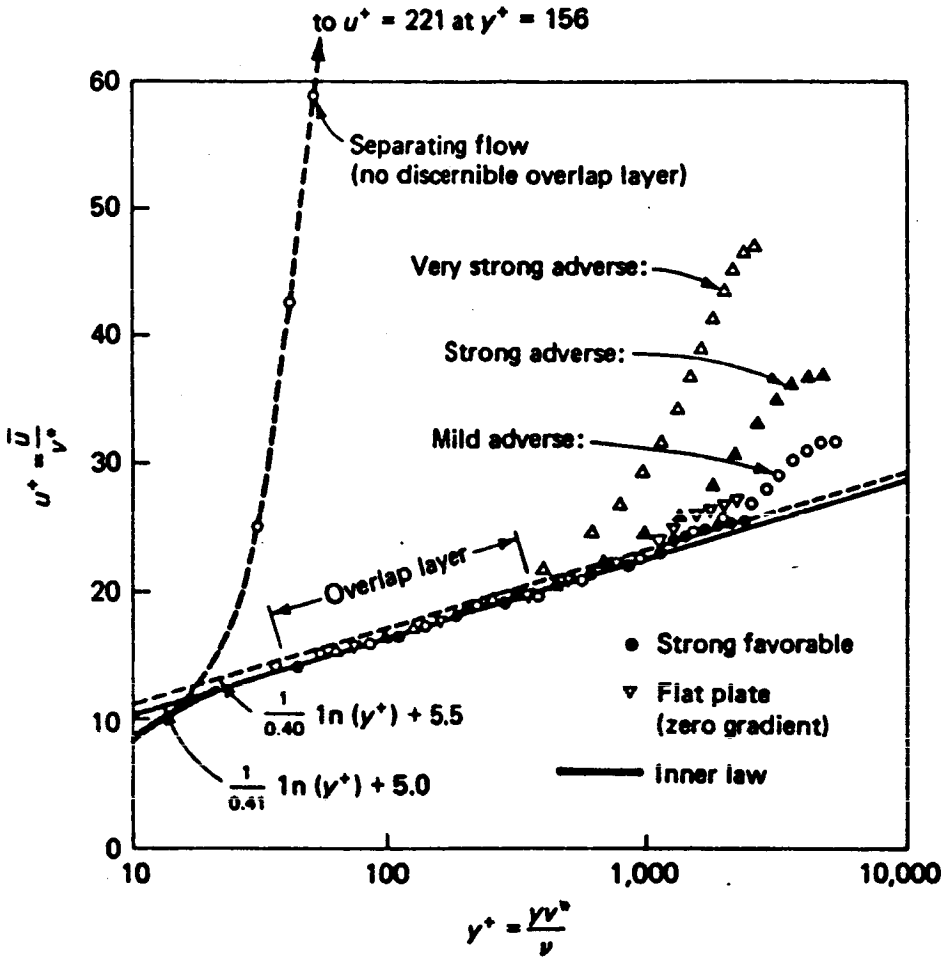

Figure 3. Turbulent boundary layer profiles for various pressure gradients using inner law variables. See e.g. reference [28].

IV
RESULTS

A total of ten CFD analyses of TAD flows within the duct configuration depicted in Figure 1 were performed using the CNS2D computer code. Three different grid discretizations were employed. A coarse 61x21 mesh was initially specified in order to determine starting estimates of the flow field characteristics. Near turn detail of this mesh configuration is displayed in Figure 5. Longitudinal refinement of this discretization was introduced using a 91x21 mesh, also displayed in Figure 5. Additional cross-stream detail was achieved using a 91x41 mesh. It was found that flow field characteristics determined using the refined meshes at significantly higher computational overhead differed only slightly (±3%) from results obtained using the coarse 61x21 discretization. Therefore, flow field properties presented in the balance of this report were obtained from computations based on the 61x21 mesh configuration.

Of the ten CFD analyses performed, seven were conducted to test the sensitivity of the turbulence models to variation in model tuning parameters (turbulence model constants). Results of these sensitivity analyses are presented at the end of this section. The remaining three analyses were conducted using specific turbulence model options available within the CNS2D computer code. A description of these options is given below.

Option 1 - designated ss k-ε, employs a conventional single scale k-ε turbulence model with the standard logarithmic law used in the wall function treatment

Option 2 - designated mwf, employs a conventional single scale k-ε turbulence model with a pressure modified wall law used in the wall function treatment

Option 3 - designated ms k-ε, employs the multiple scale k-ε turbulence model described in the previous section together with the standard logarithmic law wall function treatment

The results presented in this report were obtained using the CNS2D computer code implementation of these three turbulence model/wall function options applied to the TAD configuration displayed in Figure 1.

In all analyses, the working fluid was assumed incompressible and the molecular viscosity assumed constant. A fixed Reynolds number

value of 10^6, based on the duct width D, was specified. This particular value of the duct Reynolds number was selected in order to provide computational results for comparison with TAD experimentation in progress at Colorado State University (reference NASA contract number NAS8-36354). The target Reynolds number of this experimental program is 10^6. Unfortunately, as of this writing, results at this value of the duct Reynolds number were unavailable.

The experimental water flow facility at Colorado State consists of a TAD with a cross section aspect ratio of 10 and with a turn centerline radius to duct width ratio, R_c/D, equal to 1. The apparatus cross section is very similar to the computational configuration displayed in Figure 1. A more detailed schematic sketch of this test facility is presented in reference [26].

A fully developed turbulent duct flow inlet velocity profile, as displayed in Figure 4, was assumed for all CFD analyses. A summary of the assumed computational boundary conditions is presented below.

	ss k-ε and mwf analyses	ms k-ε analyses
Inlet u	see Figure 4	see Figure 4
Inlet v	0	0
Inlet k	2.0×10^{-3}	$k_p=k_t=1.0 \times 10^{-3}$
Inlet	$C_\mu k^{1.5}/0.03$	$\varepsilon_p = /2$, $\varepsilon_t = \varepsilon$
Outlet ∇P	0	0

$Re=10^6$

The inlet values of k and ε in the above table have been normalized by $\bar{U}^2$ and $\bar{U}^3/D$ respectively.

Results of the CFD analyses utilizing the various model options described above are presented in terms of four dependent variable measures and one independent variable phenomenological measure as listed below.

1) Normalized stream function contours ($\psi^* = \psi/[\bar{U}D]$)
2) Normalized pressure contours ($P^* = [P-P_e]/[\rho\bar{U}^2]_*$)
3) Normalized turbulent kinetic energy contours ($k^* = k/\bar{U}^2$)
4) Normalized longitudinal velocity profiles ($U^* = U/\bar{U}$)
5) Separation zone normalized size.

Predicted stream function contours using the various turbulence model options are displayed in Figure 6. A most striking phenomenological difference is exhibited in the complete absence of a downstream recirculation zone for the ss k-ε option in Figure 6a. Both the multiple-scale model and the modified wall function approach predict sizeable separation regions near the TAD exit plane.

Separation is observed to occur somewhat over 9 degrees before the exit plane is reached using a pressure modified wall law as shown in Figure 6b. Using the multiple-scale model, an even longer recirculation region is predicted, with flow separation delayed until just after the TAD exit.

The occurrence of a recirculation region, with the potential for introducing flow instability and dead zone transport effects, is a most important phenomenological event to predict. This dissimilarity in the various model predictions of an important physical phenomena presents an ideal criterion for evaluation of model capabilities in strongly curved internal flows. Application of this criterion must of course await reliable experimental data.

The pressure contours displayed in Figure 7 again highlight differences in the model predictions. Pressure recovery downstream of the TAD is predicted to occur much faster using the conventional k-ε model. In all cases, a long pressure recovery region on the order of seven duct diameters in length in the exit section is predicted. Maximum and minimum pressures, governed almost exclusively by centrifugal effects in the turn around section, are virtually identical for all the models.

The turbulent kinetic energy profiles exhibited in Figure 8 highlight the most striking difference between multiple-scale model predictions and results based on the conventional k-ε model. This difference is not evidenced in the infeed section of the duct. Within the turn, however, a substantially reduced value of the turbulent kinetic energy is determined using the multiple-scale model. A much reduced turbulent diffusivity is thus indicated when compared with the traditional k-ε model predictions. Near the duct exit plane, this difference is particularly significant, approaching a full order of magnitude reduction in ν_t.

Predicted values of the turbulent kinetic energy and diffusivity were generally somewhat less in the TAD section with the pressure modified wall law than with conventional wall functions as displayed in Figures 8a and 8b. The anamolous TAD section k contours are strongly affected by sharp mean field velocity gradients, both longitudinal and spanwise. Verification of these unusual patterns must await additional experimental evidence.

Mean longitudinal velocity profiles are presented in Figures 9, 10, and 11 for the TAD entrance, 90 degree line, and exit plane respectively. Little difference between model predictions is observed at the turn entrance and 90 degree plane, resembling in each case a potential flow profile. The multiple-scale model did, however, tend to predict lower mean velocities near the concave wall compared to the other models.

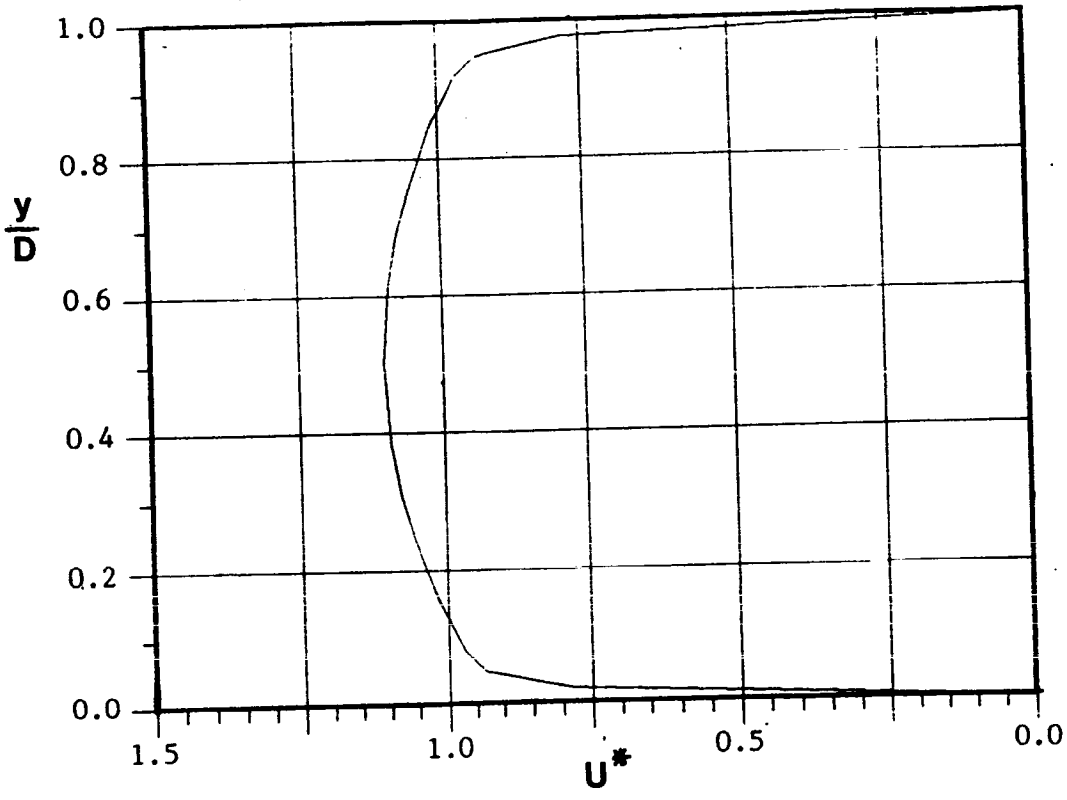

Figure 4. Inlet veclocity profile for all TAD analyses.

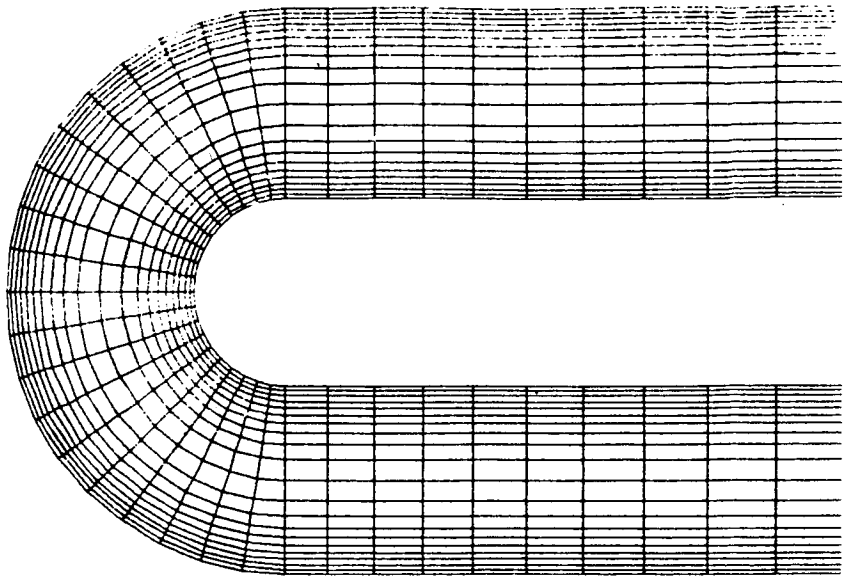

61 x 21

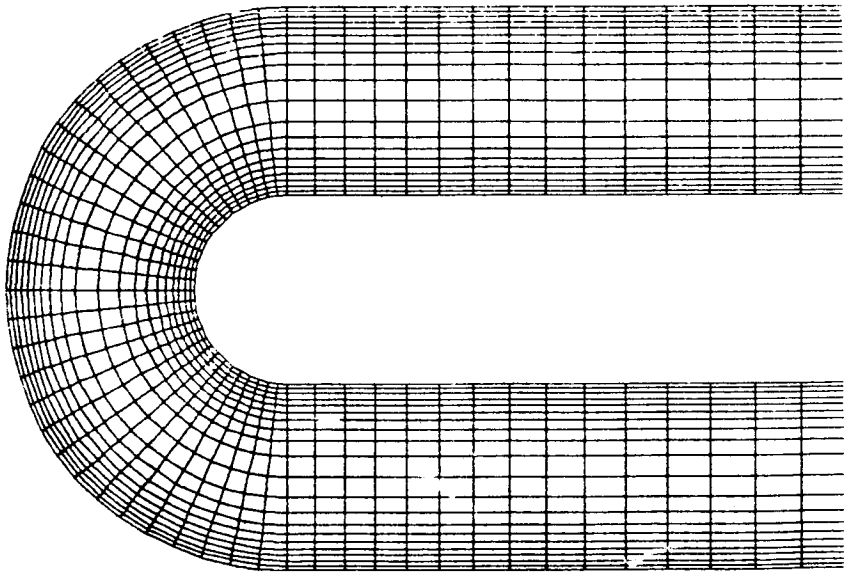

91 x 21

Figure 5. Near turn mesh configurations for TAD analyses

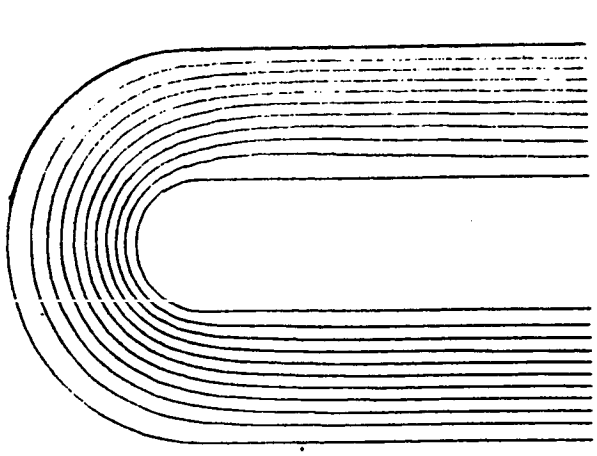

a) Single scale k-ε model with standard wall function.

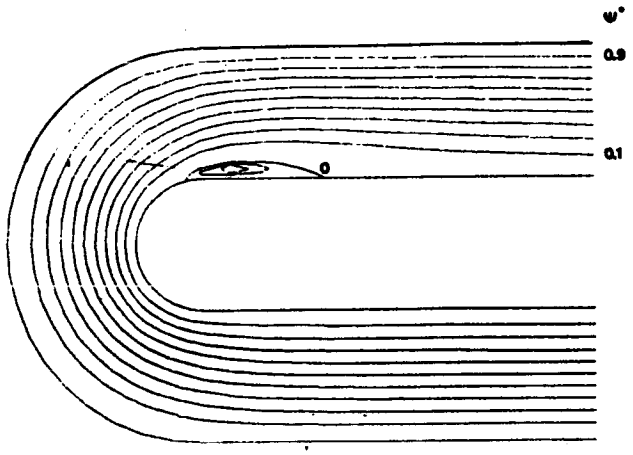

b) Single scale k-ε model with modified wall function.

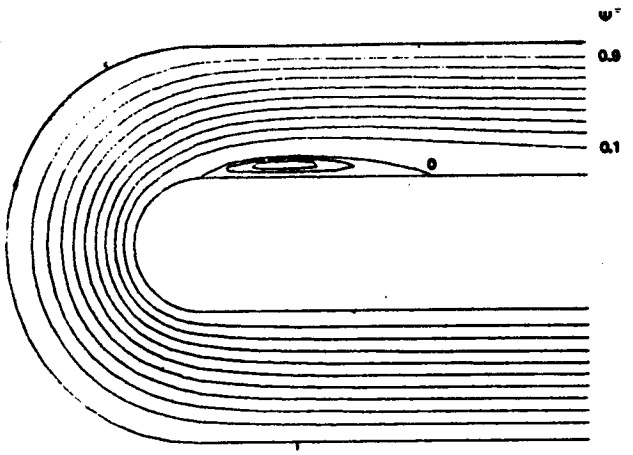

c) Multiple scale k-ε model with standard wall function.

Figure 6. Stream function contours for TAD analyses, $Re=10^6$.

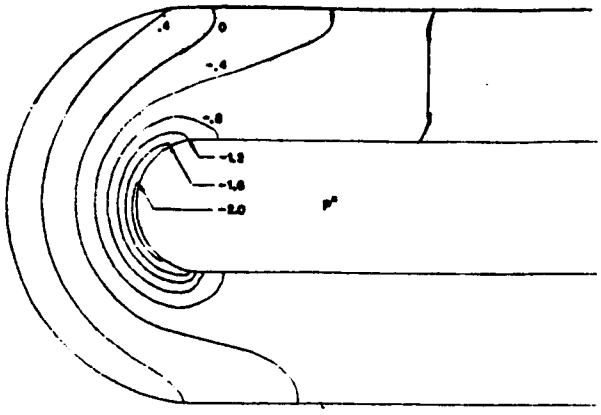

a) Single scale k-ε model with standard wall function.

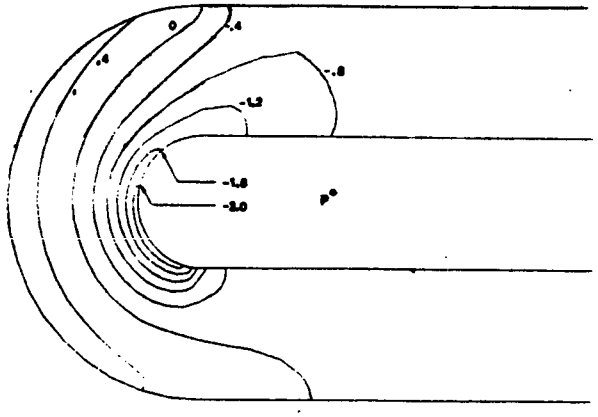

b) Single scale k-ε model with modified wall function.

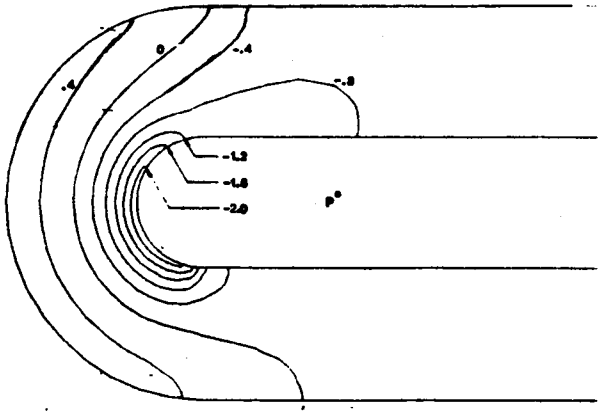

c) Multiple scale k-ε model with standard wall function.

Figure 7. Normalized pressure contours for TAD analyses, $Re=10^6$.

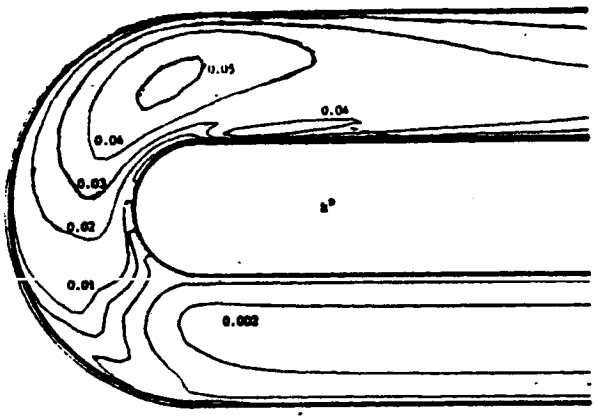

a) Single scale k-ε model with standard wall function.

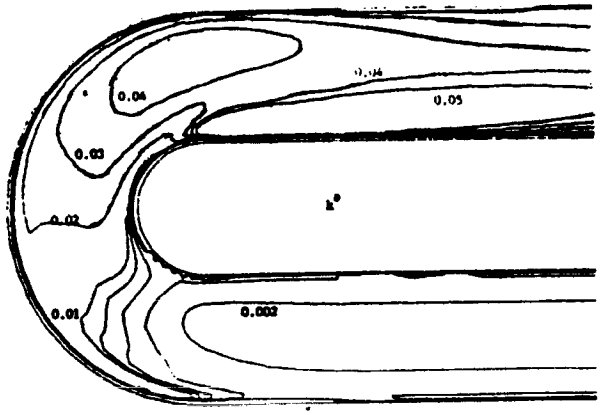

b) Single scale k-ε model with modified wall function.

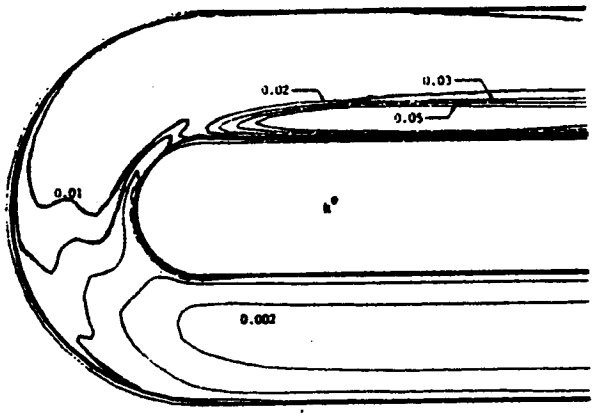

c) Multiple scale k-ε model with standard wall function.

Figure 8. Normalized turbulent kinetic energy contours for TAD analyses, Re=10^6.

Considerable variation in the mean field velocity profiles at the exit plane is displayed in Figure 11. The conventional k- model profile strongly resembles a fully developed turbulent duct flow profile at this point, evidencing an extremely fast adjustment to the approached exit section. It is well known that the k equation in the standard k-ε model exhibits an overly fast response to the mean shear stress development [9]. This process is symbiotic, effectively accelerating the mean field adjustment as evidenced in Figure 11. The profile symmetry exhibited when using the modified wall law with the k-ε model is also a reflection of this tendency for fast mean field adjustment, with exit plane recirculation causing core profile overshoot. Only the multiple-scale model results exhibit substantial profile assymmetry, indicating a retarded mean field response.

Figures 12, 13, and 14 display predicted turbulent kinetic energy profiles at the turn entrance, 90 degree plane, and exit respectively. Inlet profiles were virtually identical except near the outer wall where the modified wall function predicted a significant profile overshoot when compared with both the single-scale and split spectrum models. Previous study [26] of sharply curved TAD flows with $R_c/D = 1$ but at reduced flow rates has indicated a tendency of computational models to overpredict the turbulent kinetic energy at the turn inlet. In this regard multiple-scale model predictions exhibited no tendency for downward adjustment at $\theta = 0$ degrees, however, as evidenced in Figure 13, a significant decrease in the predicted k values was observed at the mid-turn plane. There is some experimental evidence [26] at lower Reynolds numbers to support reduced k values near the inner wall. Full k profile reduction as predicted by the multiple-scale model has not been observed. Exit plane kinetic energy profiles displayed in Figure 14 have the same general features as the midplane profiles with the exception of the modified wall function profile. The mwf approach provided substantial profile overshoot in the exit plane recirculation region. It should be observed that all model profiles exhibited in Figures 13 and 14 differ substantially from previously reported computational results and experimental observation [26] at lower Reynolds numbers.

Predicted pressure profiles at the TAD entrance and 90 degree sections were virtually identical for all the models tested as displayed in Figures 15 and 16. These profiles exhibit the predominance of a centrifugally induced cross stream pressure gradient. At the exit plane, use of the modified wall function model significantly retarded the inner wall pressure recovery while enhancing outer wall pressure relaxation as shown in Figure 17. Similar remarks apply to results based on the multiple-scale model as compared to the conventional k-ε model predictions exhibited in Figure 17. Further experimental evidence at high Reynolds numbers will be required in order to ascertain the validity of any of these significantly differing cross stream profiles.

The computational results described above highlight two striking differences in the various model results. The first is the downstream separation-reattachment region recovered using both the modified wall function approach and the split spectrum model which is absent from results based on a conventional k-ε model treatment. Although there is little current evidence to support or refute the existence of such a zone at high flow rates, the computational differences do present an effective criterion for comparative model evaluation when experimental data becomes available.

The second major difference involves the substantial reduction in turbulent diffusivity associated with use of the multiple-scale model. There exists some evidence obtained at lower Reynolds numbers to support a reduction in the turbulent kinetic energy and diffusivity in sharply curved flows [26]. Additional information is required in order to make the appropriate quantitative comparisons needed for model verification.

In addition to the basic model comparisons described above, several computational analyses were performed in order to test the sensitivity of the multiple-scale approach to the model tuning parameters, σ_k, σ_ε, C_{p1}, C_{p2}, C_{t1}, and C_{t2}. The value of each of these parameters in turn was increased 3% in order to study the effects on computational predictions. Except for C_{p1}, little variation either in the dependent variable measures or in the phenomenological recirculation zone measure was observed. A 26% increase in the length of the recirculation zone was observed upon changing C_{p1} 3% as shown in Figure 18. Values of the dependent variable were little modified anywhere except near the separation region. This is indicative of an inherent instability associated with this region. The relative insensitivity of the multiple-scale approach to other parameter variation is an indication of a robust model. Little objective evidence is available to confirm accuracy for the flow conditions tested. As with most turbulent flow computation, more experimental verification is necessary.

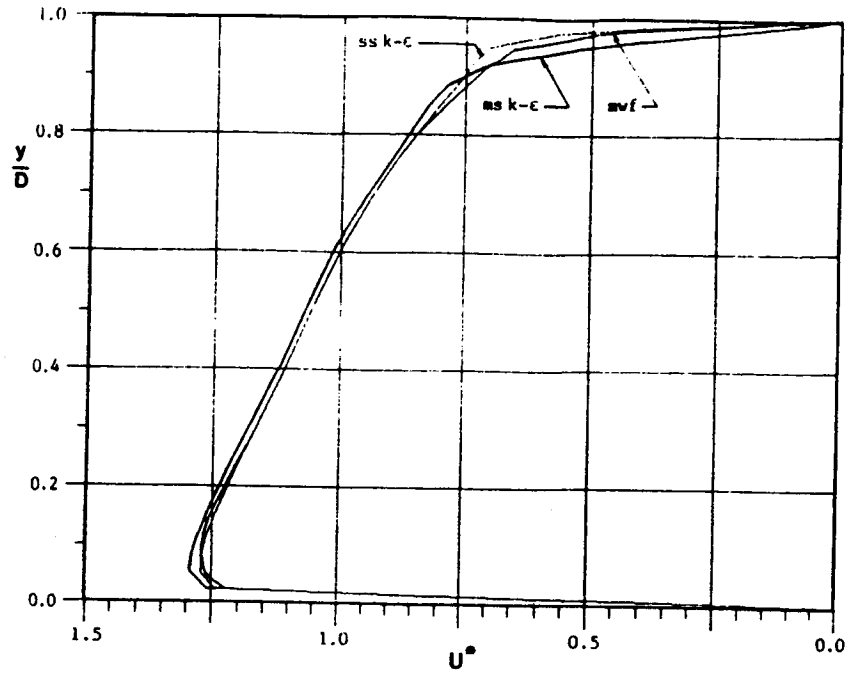

Figure 9. TAD inlet velocity profiles, Re=10^6.

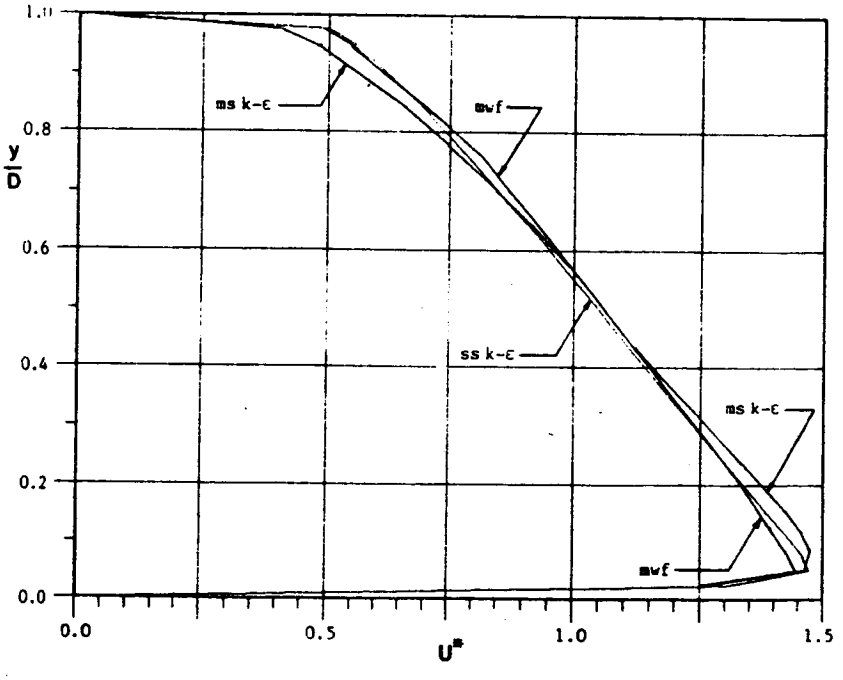

Figure 10. TAD 90° velocity profiles, Re=10^6.

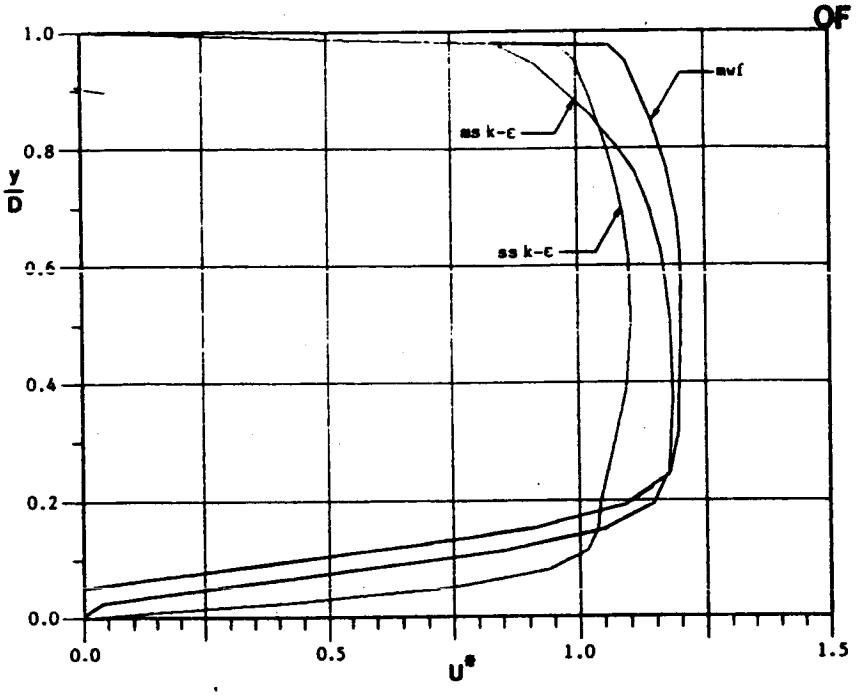

Figure 11. TAD outlet velocity profiles, Re=10^6.

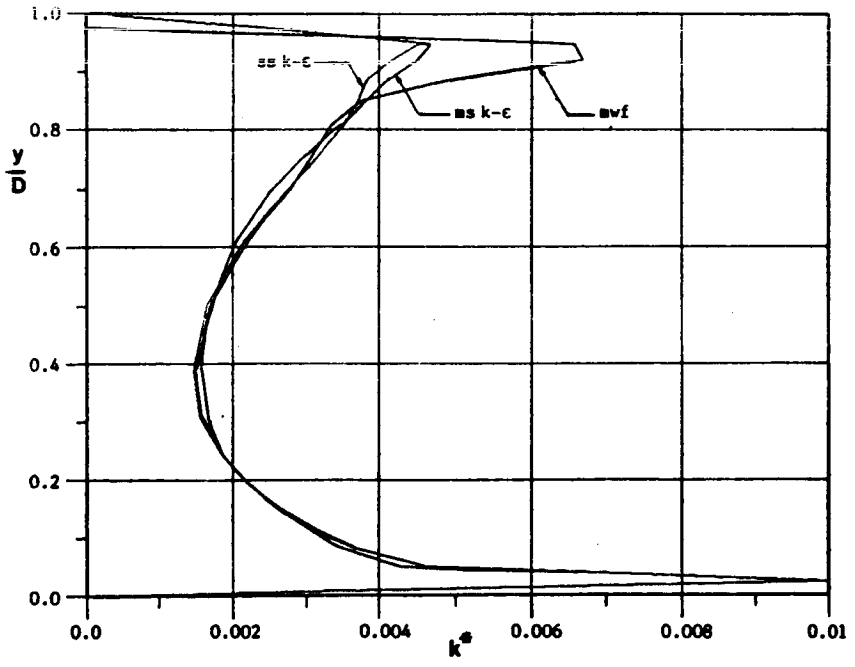

Figure 12. TAD inlet turbulent kinetic energy profiles, Re=10^6.

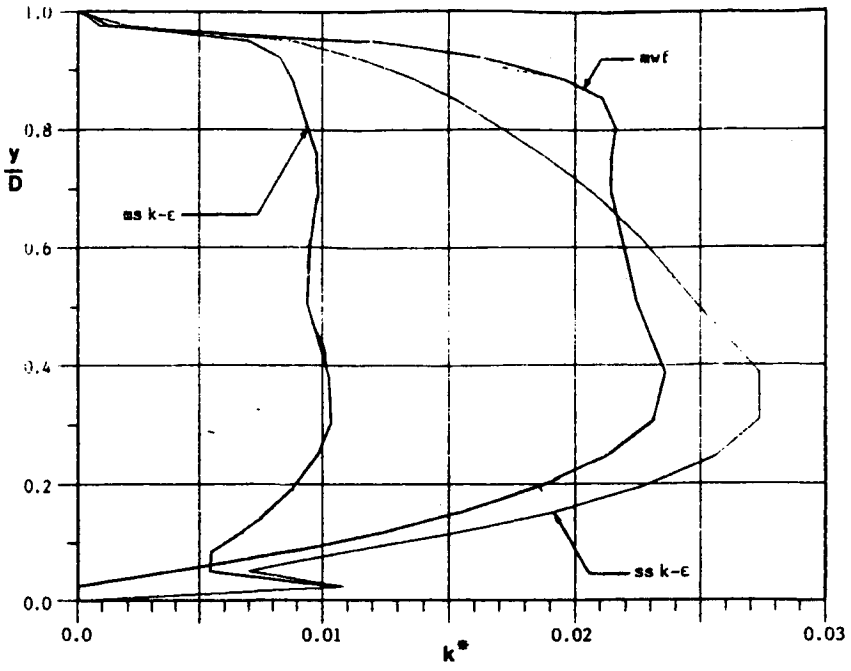

Figure 13. TAD 90° turbulent kinetic energy profiles, $Re=10^6$.

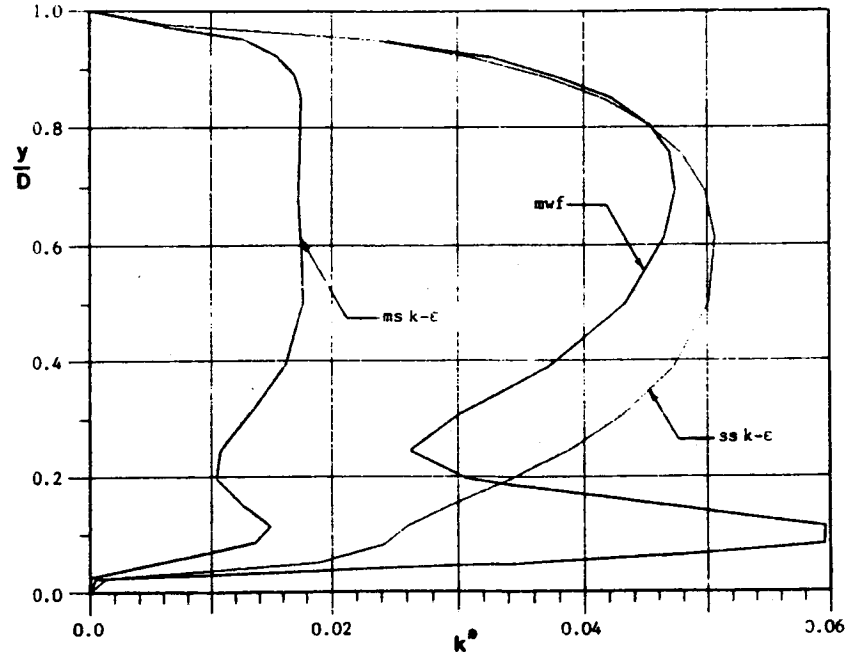

Figure 14. TAD outlet turbulent kinetic energy profiles, $Re=10^6$.

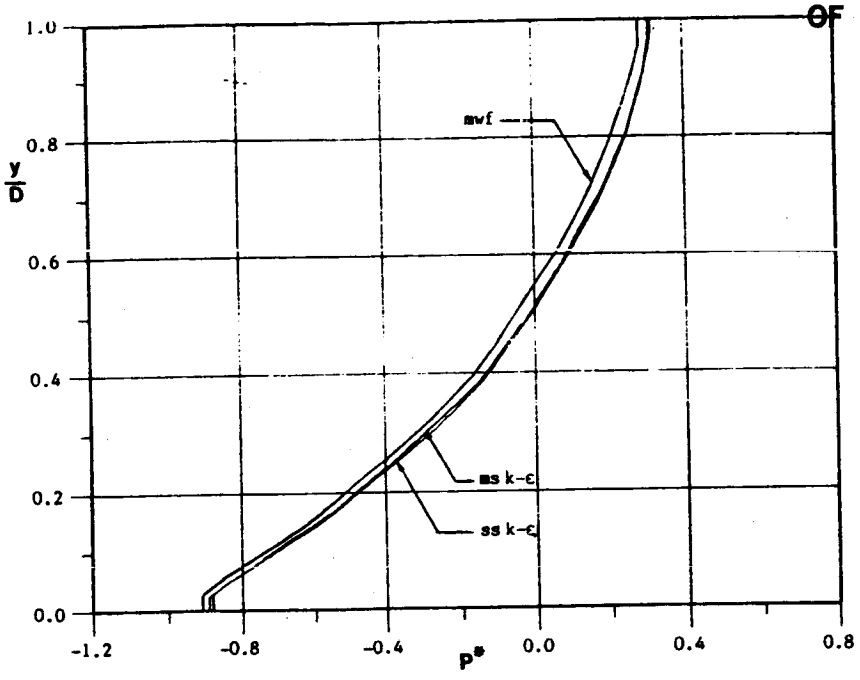

Figure 15. TAD inlet pressure profiles, Re=10^6.

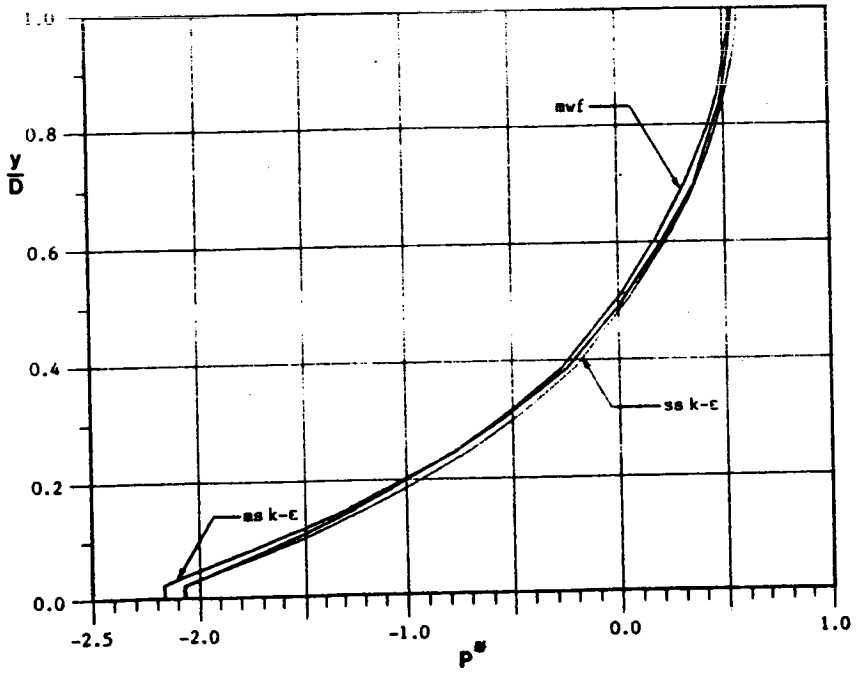

Figure 16. TAD 90° pressure profiles, Re=10^6.

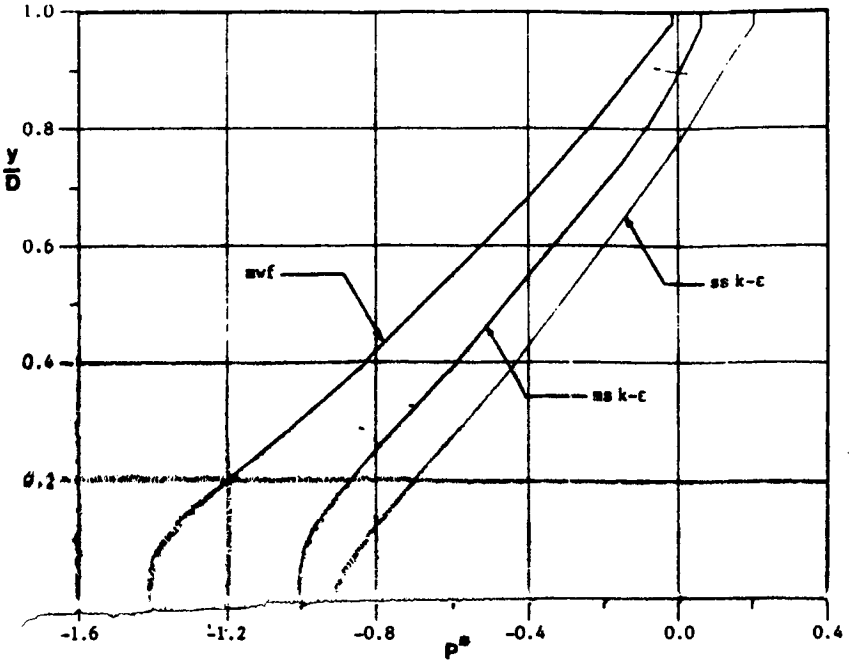

Figure 17. TAD outlet pressure profiles, Re=10^6

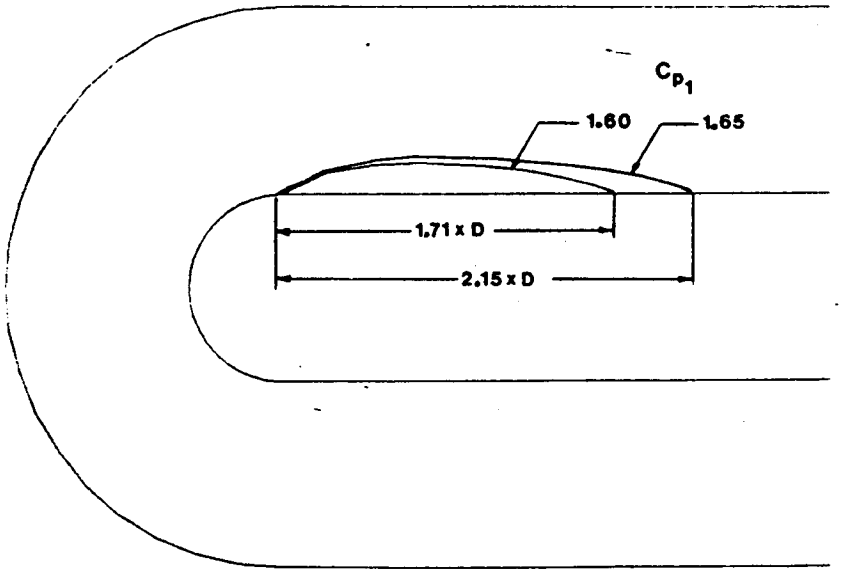

Figure 18. Multiple scale k-ε model, C_{p_1} parameter sensitivity.

V
OBSERVATIONS AND RECOMMENDATIONS

1) The CNS2D computer code provides a flexible and robust computational tool for BFC coordinate analysis.

2) At a Reynolds number of 10^6 both the multiple-scale k-ε model and the conventional k-ε model with a pressure modified wall function treatment provide TAD predictions which differ significantly from a conventional k-ε model approach using a logarithmic law wall function. Both modifications of the standard two equation model predict flow separation at the TAD exit plane, even at this elevated Re value. This is in contrast to the no separation prediction of the standard model.

3) The multiple-scale turbulence model predicts significantly reduced turbulent diffusivity in sharply curved flow regions at high Re values.

4) Both the multiple-scale k-ε model and the conventional k-ε model with pressure modified wall function treatment provide viable turbulence modeling modifications and the potential for significant model improvement with little additional computational overhead.

5) Modification of the CNS2D code to include additional production terms due to extra, curvature induced, strain should be tested.

6) A modified wall function approach appropriate to the multiple-scale k-ε model should be developed in order to simultaneously account for spectral non-equilibrium and adverse pressure gradient in sharply curved flows.

7) Additional TAD experimentation is needed in order to provide a basis for testing the applicability of improved turbulence models to sharply curved flows at very high Reynolds numbers.

REFERENCES

1. Bradshaw, P., "Effects of Streamline Curvature on Turbulent Flow," AGARDograph No. 169, 1973.

2. Launder, B. E., Pridden, C. H., and Sharma, B. I., "The Calculation of Turbulent Boundary Layers on Spinning and Curved Surfaces," Trans. ASME, Journal of Fluids Engineering, pp. 231-239, 1977.

3. Hunt, I. A. and Joubert, P. N., "Effects of Small Streamline Curvature on Turbulent Duct Flow," Journal of Fluid Mechanics, Vol. 91, pp. 633-649, 1979.

4. Humphrey, J. A. C., Whitelaw, J. H., and Yee, G., "Turbulent Flow in a Square Duct with Strong Curvature," Journal of Fluid Mechanics, Vol. 103, pp. 443-463, 1981.

5. Pourahmadi, F. and Humphrey, J. A. C., "Prediction of Curved Channel Flow with an Extended k-ε Model of Turbulence," AIAA Journal, Vol. 21, pp. 1365-1373, 1983.

6. Muck, K. C., Hoffman, P. H., and Bradshaw, P., "The Effect of Convex Surface Curvature on Turbulent Boundary Layers," Journal of Fluid Mechanics, Vol. 161, pp. 347-369, 1985.

7. Hoffman, P. H., Muck, K. C., and Bradshaw, P., "The Effect of Concave Surface Curvature on Turbulent Boundary Layers," Journal of Fluid Mechanics, Vol. 161, pp. 371-403, 1985.

8. Nakayama, A. and Koyama, H., "A Wall Law for Turbulent Boundary Layers in Adverse Pressure Gradients," AIAA Journal, Vol. 22, pp.1386-1389, 1984.

9. Chen, Y. S., "Application of a New Wall Function to Turbulent Flow Computations," AIAA paper 86-0438, AIAA 24th Aerospace Sciences Meeting, Reno, Nevada, 1986.

10. Chorin, A. J., "A Numerical Method for Solving Incompressible Viscous Flow Problems," Journal of Computational Physics, Vol. 2, pp. 12-26, 1967.

11. Vanka, S. P., Chen, B. C.-J., and Sha, W. T., "A Semi-Implicit Calculation Procedure for Flows Described in Boundary-Fitted Coordinate Systems," Numerical Heat Transfer, Vol. 3, pp. 1-19, 1980.

C-11

12. Maliska, C. R. and Raithby, G. D., "A Method for Computing Three Dimensional Flows Using Non-Orthogonal Boundary-Fitted Coordinates," International Journal for Numerical Methods in Fluids, Vol. 4, pp. 519-537, 1984.

13. Shyy, W., Tong, S. S., and Correa, S. M., "Numerical Recirculating Flow Calculation Using a Body-Fitted Coordinate System," Numerical Heat Transfer, Vol. 8, pp. 99-113, 1985.

14. Chen, Y. S., "A Numerical Method for Three-Dimensional Incompressible Flows Using Nonorthogonal Body-Fitted Coordinate Systems," AIAA paper 86-1654, 22nd Joint Propulsion Conference, Huntsville, Alabama, 1986.

15. Launder, B. E. and Schiestel, R., "Sur l'utilisation d'echelles temporelles multiples en modelisation des ecoulements turbulents," C. R. Acad. Sci., Ser. B, Vol. 286, p.709, 1978.

16. Hanjalic, K., Launder, B. E., and Schiestel, R., "Multiple-Time-Scale Concepts in Turbulent Transport Modelling," in Turbulent Shear Flow 2, L. J. S. Bradbury et al., Editors, Springer-Verlag, p. 36, 1980.

17. Hanjalic, K. and Stosic, N., "Hysteresis of Turbulent Stresses in Wall Flows Subjected to Periodic Disturbances," in Turbulent Shear Flow 4, Springer-Verlag, p.287, 1984.

18. Chen, C. P., "Multiple-Scale Turbulence Closure Modeling of Confined Recirculating Flows," NASA report CR-178536, 1985.

19. Launder, B. E. and Spalding, D. B., "The Numerical Computation of Turbulent Flows," Computer Methods in Applied Mechanics and and Engineering, Vol. 3, pp. 269-289, 1974.

20. Amano, R. S., "Development of a Turbulence Near-Wall Model and Its Application to Separated and Reattached Flows," Numerical Heat Transfer, Vol. 7, pp. 59-75, 1984.

21. Van Doormal, J. P. and Raithby, G. D., "Enhancements of the SIMPLE Method for Predicting Incompressible Fluid Flows," Numerical Heat Transfer, Vol. 7, pp. 147-163, 1984.

22. Anderson, D. A., Tannehill, J. C., and Pletcher, R. H., Computational Fluid Mechanics and Heat Transfer, McGraw-Hill, 1984.

23. Stone, H. L., "Iterative Solution of Implicit Approximations of Multidimensional Partial Differential Equations," SIAM Journal of Numerical Analysis, Vol. 5, pp. 530-558, 1968.

24. Townsend, A. A., "Equilibrium Layers and Wall Turbulence," Journal of Fluid Mechanics, Vol. 11, pp. 97-120, 1961.

25. Mellor, G. L., "The Effects of Pressure Gradients on Turbulent Flow near a Smooth Wall," Journal of Fluid Mechanics, Vol. 24, pp. 255-274, 1966.

26. Chen, Y. S. and Sandborn, V. A., "Computational and Experimental Study of Turbulent Flows in 180 Degree Bends," AIAA paper 86-1516, 22nd Joint Propulsion Conference, Huntsville, Alabama, 1986.

27. So, R. M. C., "The Effects of Extended Pressure-Strain Models on the Calculations of Complex Turbulent Flows,"in Thermal Science 16, Proceedings of the 16th Southeastern Seminar, Vol. 1, T. Nejat Veziroglu, Editor, p.153.

28. White, F. M., Viscous Fluid Flow, McGraw-Hill, 1974.